https://dx.doi.org/10.1016/j.scitotenv.2019.134095

Water-soluble low molecular weight organics in cloud water at Mt. Tai Mo Shan, Hong Kong

Wanyu Zhao [a,b,f], Zhe Wang [c,*], Shuwen Li [a,f], Linjie Li [a,f], Lianfang Wei [a,f], Qiaorong Xie a,f, Siyao Yue [a,f], Tao Li [d,g], Yiheng Liang [d], Yele Sun [a], Zifa Wang [a], Xiangdong Li [d], Kimitaka Kawamura [e], Tao Wang [d], Pingqing Fu [a,b,*]

[a] *Institute of Atmospheric Physics, Chinese Academy of Sciences, Beijing 100029, China*

[b] *Institute of Surface-Earth System Science, Tianjin University, Tianjin 300072, China*

[c] *Division of Environment and Sustainability, The Hong Kong University of Science and Technology, Hong Kong, China*

[d] *Department of Civil and Environmental Engineering, The Hong Kong Polytechnic University, Hong Kong, China*

[e] *Chubu Institute for Advanced Studies, Chubu University, Kasugai 487-8501, Japan*

[f] *College of Earth and Planetary Sciences, University of Chinese Academy of Sciences, Beijing 100049, China*

[g] *School of Environmental Science and Engineering, Shandong University, Jinan 250100, China*

* Corresponding author.

E-mail addresses: z.wang@ust.hk (Z. Wang), fupingqing@tju.edu.cn (P. Fu).

ABSTRACT

Cloud-water samples collected at the summit of Mt. Tai Mo Shan (Mt. TMS, 957 m, a.s.l.), Hong Kong in autumn 2016 and spring 2017 were measured for molecular compositions and stable carbon isotope ratios ($\delta^{13}C$) of dicarboxylic acids, oxoacids and α-dicarbonyls. Oxalic acid (C_2, 253–1680 μg L^{-1})was found as the most abundant diacid, followed by succinic acid (C4, 24–656 μg L−1) in autumn and phthalic acid (Ph, 27–363 μg L−1) in spring.

Higher concentrations of Ph (192 ± 197 μg L^{-1}) and terephthalic acid (tPh, 31 ± 15 μg L^{-1}) were observed in autumn than those in spring, illustrating the enhanced contribution from fossil fuel combustion and plastic wastes burning. Stronger correlations for the shorter chain diacids (C2–C4) with NO_3^-, $NSS - so_4^{2-}$ and nss-K^+ in autumn (R2 ⩾ 0.7) than spring suggested that these diacids were mainly produced via atmospheric photooxidation following anthropogenic emissions. The $\delta^{13}C$ values of C_2 (mean − 14.7‰), glyoxylic acid (ωC2, −12.2‰), pyruvic acid (Pyr, −15.5‰), glyoxal (Gly, −13.5‰) were much higher than those in atmospheric aerosols from isoprene and other precursors, indicating that diacids, oxoacids and α-dicarbonyls in cloud atMt. TMSwere significantly influenced by photochemical formation during the long-range atmospheric transport.

INTRODUCTION

The water-soluble dicarboxylic acids, oxocarboxylic acids and α-dicarbonyls are abundant in urban (Kawamura and Ikushima, 1993; Löflund et al., 2002; Zhao et al., 2018), mountainous (Kawamura et al., 2013; Khwaja et al., 1995; Sullivan et al., 2015; Voisin et al., 2000), marine (Hegg et al., 2002;Mochida et al., 2007) and the Arctic (Kawamura et al., 2010; Narukawa et al., 2002) atmosphere. Owing to their low vapor pressure and high hygroscopicity, diacids and related

compounds are important to increase the ability of aerosols to be cloud condensation nuclei (CCN) (Andreae and Rosenfeld, 2008; Bilde et al., 2015; Prenni et al., 2001) to affect the formation, development and dissipation processes of cloud (Dall'Osto et al., 2009; Gioda et al., 2008; Hennigan et al., 2012). High levels in concentrations of diacids and others are strongly linked to human activities (Joos and Baltensperger, 1991; Kumar et al., 2015; Myriokefalitakis et al., 2008; Wang et al., 2012) and to photochemistry (Carlton et al., 2007; Kawamura and Gagosian, 1987; Lim et al., 2010). While they are not only derived from primary sources, like marine emissions (Rinaldi et al., 2011; Tedetti et al., 2006), biomass burning (Legrand and Angelis, 1996; Narukawa et al., 1999), fossil fuel combustion and vehicular exhausts (Kawamura and Kaplan, 1987; Rogge et al., 1993), but diacids and related compounds are also largely formed via the photooxidation of organic precursors during atmospheric transport (Charbouillot et al., 2012; Hatakeyama et al., 1987; Kawamura et al., 1996).

The dicarboxylic acids and related compounds have long been considered as signature compounds to investigate the sources, photochemical aging and long-range transport of aerosol particles in the atmosphere (Kawamura and Pavuluri, 2010; Khwaja et al., 1995; Pavuluri and Kawamura, 2012). The compounds-specific stable carbon isotopic composition ($\delta^{13}C$) of dicarboxylic acids is useful to estimate the relative contribution of primary sources and photochemical formation pathways to atmospheric particles (Wang and Kawamura, 2006). Shorter carbon-chain diacids with more enrichment of 13C were attributed to the kinetic isotopic effect (KIE) for the photochemical degradation of higher carbon-number diacids (Kawamura and Bikkina, 2016). For example, many studies reported that oxalic acid is more enriched in ^{13}C than other diacids in photochemical aging processing (Aggarwal and Kawamura, 2008; Pavuluri and Kawamura, 2012; Zhang et al., 2016b). Such studies mainly focused on dicarboxylic acids in atmospheric aerosols (Wang et al., 2012;

Zhang et al., 2016b; Zhao et al., 2018), while little is known about dicarboxylic acids and their stable carbon isotopic compositions in cloud water, especially in subtropical regions such as Hong Kong (HK) where photochemical activities are very active.

Different from ground surface measurements and aerosol studies, the investigation of mountain cloud provides vital information about the influence of regional anthropogenic emissions and evolution processing on organic compounds (Herckes et al., 2013; Löflund et al., 2002; McNeill, 2015; Van Pinxteren et al., 2016). Furthermore, low molecular weight (LMW) dicarboxylic acids can be largely formed via aqueous oxidation in cloud or wet aerosol (Carlton et al., 2006; Charbouillot et al., 2012; Ervens and Volkamer, 2010; Lim et al., 2005; Lim et al., 2010; Tan et al., 2010). Mount Tai Mo Shan (Mt. TMS), the highest mountain in Hong Kong, is located along the coast of the South China Sea and is connected to the Pearl River Delta (PRD) region, China. With the development of urbanizations and industrializations, the balance between economic growth and environmental protection has become a major issue in the PRD region. The air quality of HK is affected by anthropogenic emissions from the PRD region and clean marine air mass under prevalent wind like Asia monsoon. In addition, the interactions among local circulation systems, coastal topography and synoptic forcing can also affect the accumulation of air pollutants in HK (Liu and Chan, 2002a; Liu and Chan, 2002b).

Here, we report the molecular distribution of diacids, oxoacids and α-dicarbonyls in cloud waters collected at Mt. TMS from November 2016 to April 2017. Concentrations of inorganic ions in cloud waters, air-mass backward trajectories and meteorological conditions were also discussed. Moreover, the compound-specific stable carbon isotopic compositions of dicarboxylic acids and related compounds in cloud wa- ters were investigated to better estimate the contribution of

anthropo- genic emissions, photooxidation pathways and long-range transport to organic acids in the atmosphere.

MATERIALS AND METHODS

Sample collection

A total of 24 cloud water samples associated with 13 cloud events were collected in autumn (November 9–18, 2016, n = 12) and spring (March 30–April 25, 2017, n = 12) using a singlestage Caltech Active Strand Cloud-water Collector (CASCC) at the summit of Mt. Tai Mo Shan (22.41°N,114.12°E; 957 m a.s.l.), Hong Kong. The cloud droplets were drawn into a 500 mL high-density polyethylene cylinder by a fan at a flow rate of 24.5 m^3 min^{-1} with a droplet cut-off size of 3.5 μm on theoretical 50% collection efficiency (Demoz et al., 1996). Before each sampling process, the collector was repeatedly flushed using high-purity deionized water (≥ 18 MΩ) to clean and then sealed. Field blanks were collected by high-purity deionized water before and during the sampling. It is noteworthy that the collector was shut down in rainy days.

After collection, the cloud water samples were filtered through a cellulose acetate filter of 0.45mmpore size and stored in 30–50 mL bottles of different materials according to the characteristics of compounds. For example, 20 mL of each cloud water was preserved in polyethylene bottle for analysis of inorganic ions analysis. And an aliquot of each sample (15–20 mL) was immediately added by CHCl3 solution (5–7%, v/v) to avoid microbial activities, then was stored in an amber glass bottle at 4 °C until organic analysis. Field blanks were analyzed using the same experimental procedures as samples.

115 **Dicarboxylic acid analyses**

116 The LMW diacids and related compounds in cloud waters at Mt. TMS were determined using a
117 well-established method (Kawamura and Kaplan, 1987). In brief, the cloud waters were
118 concentrated into dryness using a rotary evaporator under vacuum and then reacted with BF3/n-
119 butanol (10% − 20%) at 100 °C. The derivatives were dissolved in n-hexane and analyzed by a
120 split/splitless Agilent 6980GC/FID installed with an HP-5 column (0.2 mm × 25 m, 0.5 μm film
121 thickness). Concentrations of organic acids identified in this study were corrected for the field
122 blanks, and their recoveries were better than 85%.

123 **Measurement of isotopic composition of organic compounds**

124 The stable carbon isotopic compositions ($\delta^{13}C$) of diacids and their derivatives relative to Pee Dee
125 Belemnite (PDB) are calculated using the following equation (Kawamura et al., 2004):

$$\delta^{13}C\ (‰) = \left[\left(^{13}C/^{12}C\right)_{sample}/\left(^{13}C/^{12}C\right)_{PDB} - 1\right] \times 10^3 \qquad (1)$$

126

127 Briefly, $\delta^{13}C$ values of the esters and internal standard, measured using a Thermo Trace GC Ultra
128 coupled with a Gas Isotope Ratio MS (MAT 253) via a combustion furnace (DB-5MS: 30 m ×
129 0.25 mm × 0.25 μm) maintained at 1000 °C, were then calculated for individual organic acids on
130 the basis of the isotopic mass balance equations:

$$HOOC(CH_2)_nCOOH + 2C_4H_9OH \rightarrow H_9C_4OOC(CH_2)_nCOOC_4H_9 \qquad (2)$$

$$\delta^{13}C_{DiBE} = f_{Diacid}\delta^{13}C_{Diacid} + f_{BuOH}\delta^{13}C_{BuOH} \qquad (3)$$

131

132 The $\delta^{13}C_{DiBE}$, $\delta^{13}C_{Diacid}$, $\delta^{13}C_{BuOH}$ are the $\delta^{13}C$ values of diacid dibutyl ester, diacid and 1-butanol,
133 while f_{Diacid} and f_{BuOH} are carbon fractions in the derivatives of diacid and butanol respectively.
134 Molar fractions of original compounds carbon and butanol-derived carbon in the derivatives are

reported in detail by Kawamura et al. (2004). The δ13C values of dicarboxylic acids, oxoacids and α-dicarbonyls in cloud were corrected for the field blanks. The analytical differences in the determination of δ13C values of organic compounds based on replicate analyses were below 0.4‰.

Inorganic ions

Concentrations of cations ($NH4^+$, Na^+, K^+, Ca^{2+} and Mg^{2+}) and anions (Cl^-, NO_3^- and SO_4^{2-}) in cloud waters were measured using an ion chromatography (Dionex, Model 2500). The separation of cations was determined by an IonPac CS12A column with the eluent of methanesulfonic acid, and the separation of anions was analyzed by an IonPac AS11-HC separator column with the gradient elution of NaOH. The method detection limit for inorganic ions was 0.01 mg L^{-1}. And the detection uncertainty was below 10%.

WRF model set-up

This study utilized the Advanced Weather Research and Forecasting model (WRF, V3.6.1), coupled with a single-layer urban canopy model (UCM) to simulate the weather condition, planetary boundary layer height (PBLH) and other meteorological elements (Chen et al., 2011; Skamarock, 2008). As shown in Fig. S1, a two-ways nest was adopted for three domains of the WRF model, with horizontal grid points of 136 × 109, 136 × 121 and 133 × 109, and spatial resolutions of 9.0, 3.0, and 1.3 km. The physical parameterization schemes used in WRF domains included the Kessler microphysics scheme (Kessler, 1995), Kain-Fritsch cumulus parameterization (Kain, 2004), rapid radiative transfer model (RRTM) longwave radiation (Mlawer et al., 1997) and Dudhia shortwave radiation (Dudhia, 1989). The model time step was 52 s, and the time interval of WRF output data was 1 h.

The WRF simulations were driven by the National Centers for Environmental Prediction (NCEP) Global Final (FNL) reanalysis data with 1° × 1° spatial resolution and temporal resolution of 6 h for initial and boundary conditions. According to the sampling time, 4 case analyses (Nov09#1 during 5:30–13:00, Nov16#2 during 0:10–12:30, Nov18#3 during 16:30–22:50 and Apr21#4 during 2:30–12:30) were selected to investigate the meteorological influence on the concentration variations of organic compounds in cloud. Therefore, the periods of 4 numerical simulations covered observation time of these cases. The first 6 h of each simulation are treated as spin-up time, and the remaining hours (7–48 h) used for evaluation were corresponding to the sampling time of cloud water collected at Mt. TMS.

Air mass backward trajectories

To characterize air masses of different origins encountered the sampling site, three-day backward trajectory analyses with fire spots were conducted for each cloud water sample at the summit of Mt. TMS by using a Hybrid Single Particle Lagrangian Integrated Trajectory (HYSPLIT4) model (Rolph et al., 2017). Fire spots datasets were downloaded from the MODIS website (https://earthdata.nasa.gov/ earth-observation-data/near-real-time/firms). Each backward trajectory was drawn every hour (Fig. 1).

RESULTS AND DISCUSSION

Molecular distributions of diacids, oxoacids and α-dicarbonyls

Mass concentrations of dicarboxylic acids, oxocarboxylic acids and α-dicarbonyls in Mt. TMS cloud are listed in Table 1. The concentrations of dicarboxylic acids in autumn is dominated by oxalic acid (C2: 935 ± 440 μg L^{-1}), followed by succinic acid (C4: 250 ± 176 μg L^{-1}), malonic

178 acid (C3: 225 ± 152 μg L^{-1}) and phthalic acid (Ph: 192 ± 197 μg L^{-1}), while the order in spring is
179 C2 (418 ± 126 μg L^{-1}) N Ph (114 ± 85 μg L^{-1}) N C4 (71 ± 55 μg L^{-1}) N C3 (58 ± 28 μg L^{-1}) in
180 Fig. 2. Such a difference in autumn and spring were associated with the photochemical production
181 and the emission strength of primary sources (Cao et al., 2003; Ho et al., 2011; Lee et al., 2002;
182 Lee et al., 2001; Louie et al., 2005), like vehicular exhausts, fossil fuel combustion, marine
183 phytoplankton activities and the meteorological factor.

184 Oxalic, malonic and succinic acids, the three shortest chain diacids, had similar concentration
185 variations in sampling seasons, indicating that they were derived from common sources or
186 secondary oxidation pathways. Malonic acid can be produced by the hydrogen abstraction
187 processing of OH radical after the decarboxylation reaction of succinic acid. The C_3/C_4 ratio is
188 larger than unity in photochemically aged aerosol (Kawamura and Ikushima, 1993). Concentration
189 ratios of C_3/C_4 in this study showed similar mean values (0.93) in autumn and spring, sug- gesting
190 that atmospheric oxidation pathways largely contribute to di- acids in cloud at Mt. TMS. Adipic
191 acid (C_6) and phthalic acid are oxidation products of anthropogenic cyclic hexane (Hamilton et al.,
192 2006; Müller et al., 2007) and gaseous aromatic hydrocarbons (e.g. naphthalene) from fossil fuel
193 combustion (Kautzman et al., 2010), sol- vent usage (Na et al., 2003) and vehicular emissions
194 (Dabek- Zlotorzynska et al., 2005; Kawamura and Kaplan, 1987). In the present study, the average
195 concentrations of both C_6 (34 μg L^{-1}) and Ph (192 μg L^{-1}) in autumn were obviously higher than
196 those in spring (C_6: 6.8 μg L^{-1}, Ph: 114 μg L^{-1}), and were larger than those (C_6: 19 μg L^{-1}, Ph:
197 6.0 μg L^{-1}) in cloud waters at Austrian Alps (Limbeck and Puxbaum, 2000), which indicated that
198 abundant C_6 and Ph in Mt. TMS cloud were attributed to anthropogenic emissions, especially in
199 autumn. Kawamura and Pavuluri (2010) proposed that terephthalic acid (tPh) is an important

marker of plastic wastes burning. The lower concentrations of tPh in spring (11 μg L^{-1}) than autumn (31 μg L^{-1}) may be attributed to the more effective dilution of sea airflow.

Glyoxylic acid (ωC_2: 171 ± 132 μg L^{-1} in autumn, 59 ± 26 μg L^{-1} in spring) was the dominant oxoacid, followed by pyruvic acid (Pyr: 54 ± 37 μg L^{-1} in autumn, 25 ± 13 μg L^{-1} in spring). Glyoxal (Gly) and methylglyoxal (MeGly), the two smallest dicarbonyls in atmosphere, are oxidation products of biogenic (e.g. isoprene) (Ervens et al., 2004; Fick et al., 2004) and anthropogenic volatile organic compounds (VOCs) (e.g. aromatics) (Volkamer et al., 2001). Both dicarbonyls can ultimately produce C_2 via aqueous reactions of the intermediates like ωC_2 and Pyr with oxidants (Carlton et al., 2007; Lim et al., 2005). Mass concentrations of Gly and MeGly were 62 ± 79 μg L^{-1} and 84 ± 56 μg L^{-1} in autumn but decreased to 23 ± 16 μg L^{-1} and 35 ± 23 μg L^{-1} in spring, respectively. The enhanced concentrations of ωC_2, Pyr, Gly and MeGly in autumn were more ascribed to the substantial organic precursors emitted from vehicular exhausts, fossil fuel combustion and biomass burning under the long-range transport of prevalent wind.

Sulfate (SO_4^{2-}) is mostly produced by the oxidation of SO_2 emitted from coal-fired power plants (Hwang and Hopke, 2007), while nitrate (NO_3^-) precursors like NOx aremainly emitted fromfossil fuel combustion and motor vehicles (Liljestrand and Morgan, 1981). Non-sea-salt potassium (nss-K^+) can be viewed as a tracer of biomass burning (Andreae, 1983). Non-sea-salt sulfate (nss-SO4 2−) and nss-K^+ were calculated using the equations reported by Keene et al. (1986)): $\mathrm{nss} - SO_4^{2-}$) $=SO_4^{2-}) - 0.12 * Na^+$ and nss-K^+=$K^+ - 0.0355 * Na^+$. In this study, $\mathrm{nss} - SO_4^{2-}$, nss-K^+, NO_3^-), major diacids (C_2–C_4, Ph, tPh) and oxoacids (ωC_2, Pyr) as well as α-dicarbonyls were selected for linear correlation analyses.

In autumn (Table S1–2), strong linear relationships were observed for C_2–C_4 with tPh, $nss-SO_4^{2-}$, nss-K^+ and NO_3^- ($R^2 \geqslant 0.64$). tPh, $\omega C_2$and Pyr moderately correlated with nss-SO4 2−, nss-K+ and NO_3^- ($R_2 \geqslant 0.39$), except for Pyr with $nss-SO_4^{2-}$,. Moreover, good correlations were found between C_3, C_4, ωC_2 and Pyr with Ph ($R^2 \geqslant 0.37$). These coefficients implied that diacids and related compounds in cloud waters at Mt. TMS were formed via secondary oxidation after atmospheric longrange transport of anthropogenic emissions (Ho et al., 2006; Huang et al., 2014; Zhang et al., 2016a), such as coal-fired power plants, vehicular exhausts, fossil fuel combustion and biomass burning.

As for springtime samples (Table S3–4), C_2, C_3, C_4 and MeGly showed robust linear correlations with nss-K^+ ($R^2 \geqslant 0.85$), while relatively weak correlations were obtained for C_3 and MeGly with NO_3^- ($R^2 \geqslant 0.39$). Previous studies proposed that open wastes burning aerosols also contain biomass and fuel burning compounds (Akagi et al., 2011; Lei et al., 2012). tPh correlated well with MeGly ($R^2 = 0.35$) and Gly ($R^2 = 0.66$) in autumn and spring, respectively. These relationships may be interpreted as the decreased anthropogenic emissions and enhanced contribution from natural sources (Guo et al., 2007; Ho et al., 2011), like marine emissions, to diacids in spring.

Oxalic acid, the smallest diacid, is mostly formed via the atmospheric oxidation of homologous dicarboxylic acids and related precursors, hence the concentration ratio of C_2 to total normal saturated diacids (C_2/C_2–C_{12}) is a useful tracer to estimate photochemical aging level of organic compounds (Kawamura and Sakaguchi, 1999). The larger value of C_2/C_2–C_{12} was observed in spring (0.73) than that in autumn (0.62), which showed an increased photooxidation level of dicarboxylic acids in Mt. TMS cloud in spring. Inversely robust correlations were observed for concentrations of main water-soluble organic acids with C_2/C_2–C_{12} ratios in this study.

Fig. 3 showed strong anti-correlations between C_3 ($R^2 \geqslant 0.56$), C4 ($R^2 \geqslant 0.49$), C_5 ($R^2 \geqslant 0.65$), C_6 ($R^2 \geqslant 0.47$) and C_2/C_2–C_{12} ratios in both sea- sons, whereas relatively weak coefficients were found for C_9 with C_2/C_2–C_{12} ($R^2 \geqslant 0.31$). These results suggested that the photochemical degradation rates of saturated long-chain diacids may be faster than their formation rates during the atmospheric long-range transport. Similarly, inverse linear relationships were found for ωC_2 ($R^2 \geqslant 0.69$), Pyr ($R^2 \geqslant 0.65$), Gly ($R^2 \geqslant 0.4$) and MeGly ($R^2 \geqslant 0.31$) with C_2/C_2–C_{12} ratios as well, which implied that photochemical oxidations of ωC_2, Pyr and dicarbonyls in aqueous phase largely contributed to the concentrations of C_2. Combined the conclusions illustrated above, we found that dicarboxylic acids and related compounds were mainly formed by the photooxidation of organic precursors derived from vehicular emissions, fossil fuel combustion and biomass burning in autumn, whereas the contribution of natural sources to dicarboxylic acids enhanced in spring. But it is critical to note that longer-chain diacids and other precursors were significantly oxidized to produce C_2 via subsequent reactions under strong solar radiation in both seasons.

Case analyses

The special conditions of terrain, small- and meso-scale atmospheric circulations, such as mountain-valley and land-sea breezes, frequently occur at Mt. TMS in HK, which increase the mixing level of polluted urban air and mountain air (Wang et al., 2016). Hence, combined with the sampling time, four case analyses (Nov09#1 during 5:30–13:00, Nov16#2 during 0:10–12:30, Nov18#3 during 16:30–22:50 and Apr21#4 during 2:30–12:30) were selected to investigate the meteorological influence on the concentration variations of organic compounds in Mt. TMS cloud. This study utilized the Advanced Weather Research and Forecasting model (WRF, V3.6.1), coupled with a single-layer urban canopy model (UCM) to simulate the synoptic circulation

situation on a small scale. The high-resolution mesoscale WRF model can accurately reflect nonlinear dynamics, thermodynamics, and microphysical process, and recur the complex synoptic processes (Done et al., 2004; Li and Bou-Zeid, 2013; Noble et al., 2013; Schwartz, 2014). Therefore, the WRF model is a useful tool to reproduce the weather condition, planetary boundary layer height (PBLH, see Fig. S2) and other meteorological elements.

Generally, the PBLH at Mt. TMS in daytime enhanced with the in- crease of temperature, which was higher than the PBLH values in night- time (Fig. S2). But the water vapor rise and condense owing to abundant moisture in air and the uplift effect of mountain (Markowski and Richardson, 2010). Rainy day often occurs at Mt. TMS, resulting in the lower PBLH at many times. Both maximum (1200 m) and minimum (60 m) of PBLH in autumn and spring were observed in daytime (av. 480 m), while the nighttime value (av. 340 m) varied from 115 m to 720 m. Thus, the cloud waters at Mt. TMS were mostly sampled in the lower free troposphere.

As shown in Figs. 4–7, owing to the lifting effect by terrestrial land and mountain, there was a convergence zone at the top of Mt. TMS (red point) in Hong Kong (Mass, 1981; Mass and Dempsey, 1985). Topographic height (units: m) of HK and surrounding areas are colorfully shaded. Meanwhile, wind field (vectors, units: m s−1) and divergence field (blue lines, units: 10^{-4} s^{-1}) are set on the summit of Mt. TMS. Horizontal divergence is defined as $D = \frac{\partial u}{\partial x} + \frac{\partial v}{\partial y}$ (u: zonalwind, v: meridional wind, x: zonal grid distance, y: meridional grid distance). If $D > 0$, it means horizontal divergence of wind field, which indicates the expansion of a vector field. The larger value of D represents the stronger outflow (Markowski and Richardson, 2010). But if $D < 0$, it indicates horizontal convergence of wind field, which indicates the contraction of a vector field. The lower value of D represents the stronger inflow (Markowski and Richardson, 2010). Mathematically, convergence is negative divergence. The lower negative value observed at sampling site

demonstrated that the stronger level of convergence occurred in this area, which facilitates the accumulation of air pollutants (Markowski and Richardson, 2010). For example, the convergence (−5) in Nov09#1 and Nov16#2 at Mt. TMS was the strongest in this study (Figs. 4–5). The level of central convergence zone was stronger in Nov18#3 than that in Apr21#4, because the negative value of contour line (−3) close to Mt. TMS was lower in Nov18#3 (Figs. 6–7).

As shown in Fig. 1, three-day backward trajectories for cloud waters collected at Mt. TMS were mainly from the Pacific Ocean and the South China Sea in autumn and spring. But according to the helical air mass backward trajectories in autumn, the marine atmosphere was largely influenced by the continental air outflow. Meanwhile, the specific three-day backward trajectories were also categorized for the cloud cases in this study (Figs. S3–6). The winds in Nov09#1 and Nov16#2 were mostly from the Pacific Ocean based on WRF model results (Figs. 4-5), but the winds came from inland area in view of large-scale situation (Figs. S3–4). As to Nov18#3, the cloud waters at Mt. TMS were totally affected by easterly sea-breeze (Fig. 6 and Fig. S5). The concentrations of organic acids were larger in Nov09#1 and Nov16#2 than those in Nov18#3 (Fig. 8), which were attributable to the strongest con- vergence and air mass sources in the atmosphere.

In late autumn and winter, the Siberian high pressure system is one of the major seasonal atmospheric activity centers in the northern hemisphere, which strongly affects the Asia continent by continuing to spread cold air mass southwards (Chan et al., 2010; Chung et al., 1999; Wang et al., 1998). Hong Kong is mainly affected by north- easterly synoptic flow from the inland region in autumn. The diacids and related compounds were more abundant in downwind location of Hong Kong in the atmospheric long-range transport. Owing to the large-scale subsidence under the control of Siberian high pressure system, the air masses from the northern China are cold and dry, which impact the atmospheric quality in HK by carrying substantial air pollutants (Chan et al.,

311 2010; Chung et al., 1999; Wang et al., 1998). Furthermore, the convergence zone at Mt. TMS in
312 lower free troposphere generally connects with a divergence zone in the upper free troposphere.
313 Then the rising air from the lower level and the sinking air from the upper level converge in the
314 free troposphere. This kind of atmospheric three- dimensional circulation system is favorable for
315 the accumulation of pollutants over Mt. TMS in HK.

316 In spring, there is the Subtropical High over the Western Pacific Ocean, which brings clean and
317 moist airflow to southern China under the East Asia monsoon (Ding, 2005; Ding et al., 2018). The
318 lower concentrations of diacids and related compounds in spring than autumn were attributed to
319 the upwind sampling location. The local emissions were diluted by the south-easterly and south-
320 westerly airflows from the South China Sea (Fig. 1b). In Apr21#4, the organic compounds in cloud
321 waters were influenced by marine emissions (Fig. S6), and Mt.

322 TMS was observed to be located at the rim of convergence zone (Fig. 7). Corresponding to the
323 highest concentrations of organic acids in the mid- day on April 4th, the convergence also showed
324 the strongest level. In total, concentrations of total diacids, oxoacids and α-dicarbonyls in these
325 cases increased with solar radiation, indicating that photochemical processing is an important
326 formation pathway for organic acids.

327 Table 2 shows the stable carbon isotope ratios of nine diacids (C_2–C_6, C_9, M, Ph and tPh), two
328 oxoacids (Pyr and ωC_2) and one dicarbonyl (Gly). The $\delta^{13}C$ values of normal saturated diacids
329 increased with the decrease of carbon numbers of dicarboxylic acids in cloud waters over Mt. TMS
330 (Fig. 9). In sum, the largest average $\delta^{13}C$ values were observed for C_2 (autumn: −18.2‰, spring:
331 −11.2‰), followed by C_3 (autumn:−19.8‰, spring: −17.1‰) and C_4 (autumn: −23.7‰,
332 spring:−20.5‰) diacids, implying that shorter diacids were more photochemically aged.

C_5 and C_6 are formed via the oxidation of anthropogenic cyclic alkenes (Hamilton et al., 2006; Müller et al., 2007) and longer-chain homologous diacids (Kawamura and Ikushima, 1993). Both $\delta^{13}C$ values (C_5: −32.2‰ to −22.1‰, C_6: −31.6‰ to −20.2‰) widely varied in au- tumn and spring owing to the complex controlling factors of isotope fractionation in the atmosphere. Similar seasonal mean $\delta^{13}C$ values (autumn: −26.4‰, spring: −25.5‰) was determined for C_9, being higher than those of fatty acids (−36.4‰ to −34.9‰) emitted from terrestrial C_3 plants (Matsumoto et al., 2007), but being close to fatty acids (−25.8‰) measured in aerosols collected from Chichijima Island over the western North Pacific (Fang et al., 2002). These phenomena suggested that C9 was produced by the secondary oxidation of unsaturated fatty acids derived from biomass burning, marine emissions and terrestrial higher plants.

Ph and its precursors are mainly emitted from fossil fuel combustion and vehicular exhausts (Fraser et al., 2003; Kleindienst et al., 2012). tPh is a tracer of plastic wastes burning (Kawamura and Pavuluri, 2010). Mean $\delta^{13}C$ value of Ph in autumn (−29.0‰) was similar to spring (−28.5‰). These values were close to those (−28.5‰) in Beijing winter aerosols associated with substantial coal combustion for house heating (Zhao et al., 2018). Same phenomenon was also observed for tPh. The similar $\delta^{13}C$ values of Ph and tPh suggested a similar stable isotopic signature for dicarboxylic acids from vehicular emissions, fossil fuel combustion and plastic wastes burning in Mt. TMS cloud waters.

Hydrated Gly (autumn: −16.6‰, spring: −10.3‰) and MeGly formed via the photooxidation of biogenic and anthropogenic VOCs can subsequently produce ωC_2 (autumn: −13.7‰, spring: −10.7‰) and Pyr (autumn: −17.2‰, spring: −13.8‰), and ultimately generate C_2 (Ervens et al., 2004; Lim et al., 2005). The $\delta^{13}C$ values of organic mat- ter from terrestrial higher plants (C_3 plants: −27‰) (Ballentine et al., 1998) are larger than those from fossil fuel combustion (Widory et al.,

2004), but lower than those of marine biological origins (around −20‰) (Turekian et al., 2003). These results indicated that Pyr, ωC_2 and α-dicarbonyls were formed via the oxidation of pre-aged precursors like isoprene and unsaturated fatty acids. It is of importance to state that besides motor vehicles and atmospheric photochemical oxidations, diacids and related compounds were more associated with fossil fuel combustion, while the contribution of marine emissions to dicarboxylic acids increased in spring. Thus, stronger enrichment of 13C was detected for C_2, ωC_2, Pyr and Gly in spring than autumn.

Implications of enriched ^{13}C in organic acids in cloud water and aerosol

To better understand the differences in $\delta^{13}C$ values of organic acids in cloud water and aerosol, the data in aerosols collected from Gosan, Jeju Island (Zhang et al., 2016b), tropical India (Pavuluri et al., 2011) and Sapporo, Japan (Aggarwal and Kawamura, 2008), the western Pacific and Southern Ocean (Wang and Kawamura, 2006) were plotted here together with $\delta^{13}C$ values of organic compounds identified in Mt. TMS cloud (Fig. 10). A slightly higher average $\delta^{13}C$ value of C_2 (−11.2‰) was observed in Mt. TMS cloud in spring. Except for Gosan aerosols, seasonal mean $\delta^{13}C$ values of C_3 diacid in Mt. TMS cloud waters were larger than those in other three sites. The mean $\delta^{13}C$ value of C_4 di- acid in spring were comparable to those in aerosol studies selected in this study. The air masses encountered at Gosan, Sapporo and remote marine area are mixed outflows from the Asia mainland, where diacids were intensively photochemically aged in the atmospheric long-range transport. These comparisons suggested that lower carbon number di-carboxylic acids were significantly photochemically aged in Mt. TMS cloud. Mean $\delta^{13}C$ values of M also supported the same conclusion.

Biomass burning, terrestrial higher plants and marine phytoplankton emissions are the major contributors to C_9 diacid in coastal urban aerosols in Sapporo, Japan (Aggarwal and Kawamura,

2008) and Chennai, topical India (Pavuluri et al., 2011). In this study, mean $\delta^{13}C$ values of C_9 were lower than those in remote marine aerosols influenced by phytoplankton activities. But $\delta^{13}C$ values of C_9 were slightly larger than those in other locations. Such phenomena suggested that azelaic acid in Mt. TMS cloud water were linked with natural biogenic emissions and biomass burning. $\delta^{13}C$ values of C_6 and Ph were lower than those in Gosan and remote marine aerosols, demonstrating that the dicarboxylic acids were partly de- rived from anthropogenic emissions, like local vehicle exhausts.

Higher $\delta^{13}C$ values were identified for ωC_2, Pyr and Gly in comparison to those in aerosol studies (Aggarwal and Kawamura, 2008; Pavuluri et al., 2011; Wang and Kawamura, 2006; Zhang et al., 2016b). Similar 13C enrichment in C_2, ωC_2, Pyr and Gly supported that these organic acids may have common secondary formation ways as found in laboratory and modelling experiments (Pavuluri and Kawamura, 2012). The $\delta^{13}C$ values of C_2, ωC_2, Pyr might indicate that uptake of semi-volatile organic compounds (Gly, MeGly) by cloud droplet and wet aerosol, followed by the oxidation of oxoacids (ωC_2, Pyr) and later evaporation is an important pathway to C_2 (Carlton et al., 2009; Ervens et al., 2004; Ervens and Volkamer, 2010; Rinaldi et al., 2011).

SUMMARY AND CONCLUSIONS

Current knowledge on molecular distribution and compound-specific stable carbon isotopic composition of dicarboxylic acids in cloud waters, as well as potential factors controlling their atmospheric abundance at a small or large scale above the planetary boundary layer based on observations is very limited. Owing to the development of urbanizations and industrializations in the PRD region, HK that is situated at the rim of the PRD region is significantly influenced by

anthropogenic emissions under prevalent winds. The top of Mt. TMS, HK is mostly observed in the upper PBL in daytime and viewed in the lower free troposphere in nighttime. Our results demonstrate that high loadings of diacids and related compounds in cloud waters at Mt. TMS in autumn are mainly attributed to anthropogenic sources, including fossil fuel combustion and biomass burning, from regional areas, whereas marine emissions play a significant role to organic acids in spring. It is worthy to note that photochemical formation during atmospheric transport and vehicular exhausts from ground surface are also important factors to dicarboxylic acids in cloud water at Mt. TMS. Further- more, this work highlights the potential influence of meteorological factors on the concentrations, molecular compositions, and δ13C values of dicarboxylic acids.

ACKNOWLEDGMENTS

This work was supported the National Natural Science Foundation of China (Grant Nos. 41625014 and 41505103), and Research Grants Council of Hong Kong SAR, China (Grant Nos. 25221215, 15265516, T24-504/17-N). The authors would like to thank Yaru Wang, Lingyan Kang, Steven Poon and Bobo Wong for their support during the cam- paign, and to thank Hong Kong Environmental Protection Department (HKEPD) for providing the facilities at the Tai Mo Shan station.

Appendix A. Supplementary data

Supplementary data to this article can be found online at https://doi.org/10.1016/j.scitotenv.2019.134095.

LIST OF TABLES AND FIGURES

Table 1

Concentrations (μg L^{-1}) of dicarboxylic acids, oxoacids and α-dicarbonyls in cloudwaters collected over Mt. TMS in Hong Kong.

Compounds (Abbr.)	Autumn ($n = 12$)		Spring ($n = 12$)	
	Range	Mean/SD	Range	Mean/SD
Dicarboxylic acids				
Oxalic, C_2	270–1680	935/440	253–694	418/126
Malonic, C_3	52–512	225/152	19–120	58/28
Succinic, C_4	55–656	250/176	24–225	71/55
Glutaric, C_5	16–154	63/47	3.7–39	14/12
Adipic, C_6	11–73	34/20	2.4–27	6.8/11
Pimelic, C_7	5.0–20	12/6.1	1.2–8.3	4.0/2.4
Suberic, C_8	4.1–15	9.2/3.3	BDL–9.2	3.2/3.5
Azelaic, C_9	6.5–30	15/7.2	2.5–14	7.5/4.1
Decanedioic, C_{10}	BDL–4.9	1.9/1.7	BDL–2.3	0.3/0.7
Undecanedioic, C_{11}	BDL–5.4	0.7/1.7	BDL	BDL
Dodecanedioc, C_{12}	BDL	BDL	BDL	BDL
Methylmalonic, iC_4	1.4–21	6.1/5.3	BDL–11	2.9/3.2
Methylsuccinic, iC_5	6.5–68	30/19	4.4–27	12/7.5
2-Methylglutaric, iC_6	2.0–16	5.9/4.0	BDL–14	4.8/4.6
Maleic, M	15–108	57/33	4.6–97	25/28
Fumaric, F	3.6–23	16/8.1	1.7–14	5.6/3.3
Methylmaleic, mM	13–81	42/23	7.7–32	17/8.8
Phthalic, Ph	49–363	192/197	27–299	114/85
Isophthalic, iPh	3.3–21	8.6/5.3	1.8–12	5.8/3.2
Terephthalic, tPh	14–65	31/15	4.0–24	11/6.7
Malic, hC_4	BDL–11	4.5/3.1	BDL–12	3.9/4.5
Oxomalonic, kC_3	2.0–63	17/17	3.5–22	10/5.6
4-Oxopimelic, kC_7	6.0–57	20/15	2.9–13	6.1/3.1
Total diacids	546–3940	1980/1050	497–1230	805/330
Oxocarboxylic acids				
Pyruvic, Pyr	12–128	54/37	7.1–39	25/13
Glyoxylic, ωC_2	33–442	171/132	19–116	59/26
3-Oxopropanoic, ωC_3	8.6–24	14/5.1	1.7–14	6.5/3.8
4-Oxobutanoic, ωC_4	BDL–24	9.6/7.3	1.2–10	4.6/2.8
5-Oxopentanoic, ωC_5	1.0–4.1	2.3/0.9	BDL–2.8	1.1/0.9
7-Oxoheptanoic, ωC_7	BDL–16	7.4/4.7	BDL–6.6	3.4/2.1
8-Oxooctanoic, ωC_8	BDL–15	6.7/4.0	BDL–4.0	1.5/1.5
9-Oxononanoic, ωC_9	2.1–13	6.3/3.4	BDL–6.6	1.9/1.7
Total oxoacids	9.5–282	272/181	36–196	102/44
α-Dicarbonyls				
Glyoxal, Gly	3.8–232	62/79	2.4–55	23/16
Methylglyoxal, MeGly	26–217	84/56	8.4–53	35/23
Total dicarbonyls	30–449	145/131	17–121	58/33

BDL: below detection limit. BDL is ca.0.05 μg L^{-1}.

Table 2

Stable carbon isotopic compositions (δ13C, ‰) of major compounds in cloud at Mt. TMS.

Compounds	Autumn (n = 12)			Spring (n = 12)		
	Min	Max	Mean ± SD	Min	Max	Mean ± SD
C_2	−24.5	−12.8	−18.2 ± 3.7	−17.8	−6.4	−11.2 ± 4.3
C_3	−22.7	−14.5	−19.8 ± 2.5	−22.7	−10.1	−17.1 ± 3.9
C_4	−29.1	−21.2	−23.7 ± 2.2	−25.7	−10.7	−20.5 ± 4.3
C_5	−29.6	−26.8	−28.2 ± 2.0	−32.2	−22.1	−26.4 ± 5.3
C_6	−31.6	−23.4	−27.3 ± 4.1	−26.6	−20.2	−23.8 ± 2.6
C_9	−27.6	−22.1	−26.4 ± 2.6	−31.4	−21.7	−25.5 ± 3.1
M	−19.6	−10.8	−15.7 ± 4.4	−22.6	−16.3	−20.8 ± 3.1
Ph	−31.2	−24.7	−29.0 ± 1.8	−32.7	−25.6	−28.5 ± 2.2
tPh	−31.1	−25.6	−29.0 ± 2.2	−33.4	−24.2	−28.8 ± 6.6
ωC_2	−26.2	−1.6	−13.7 ± 6.7	−25.4	−1.8	−10.7 ± 8.2
Pyr	−28.9	−10.0	−17.2 ± 4.7	−17.8	−4.6	−13.8 ± 4.4
Gly	−24.3	−12.9	−16.6 ± 4.3	−19.3	−4.8	−10.3 ± 5.7

SD, standard deviation.

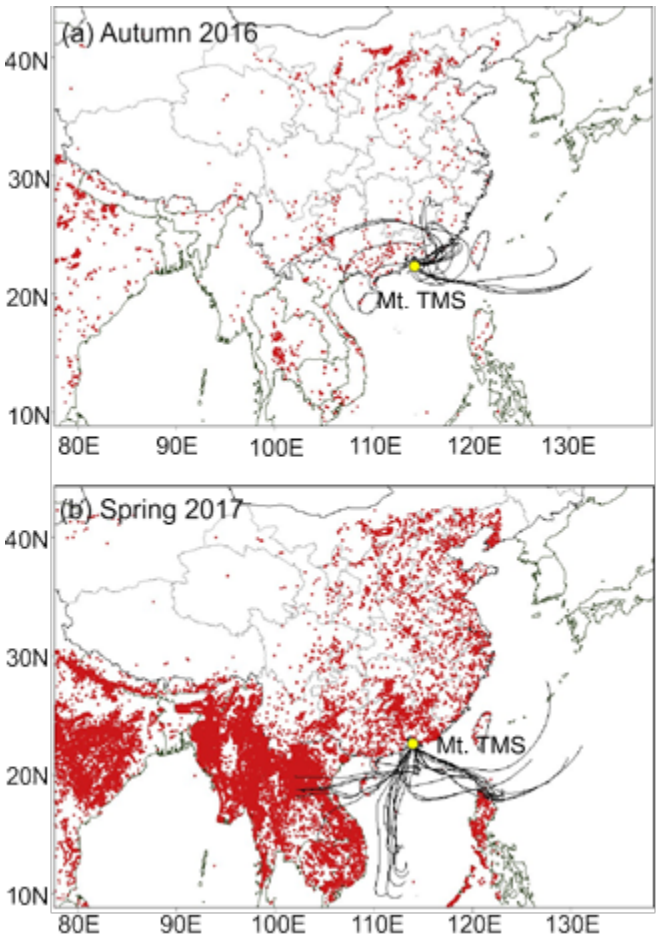

Fig. 1. Fire spots with typical 3-day air mass backward trajectories arriving at the summit of Mt. TMS in the autumn of 2016 and the spring of 2017. The fire spot data were obtained from the MODIS fire spot website (https://earthdata.nasa.gov/earth-observation-data/ near-real-time/firms). The air mass trajectories were drawn using the data obtained by the HYSPLIT4 model from the NOAA ARL website (http://ready.arl.noaa.gov/ HYSPLIT. php).

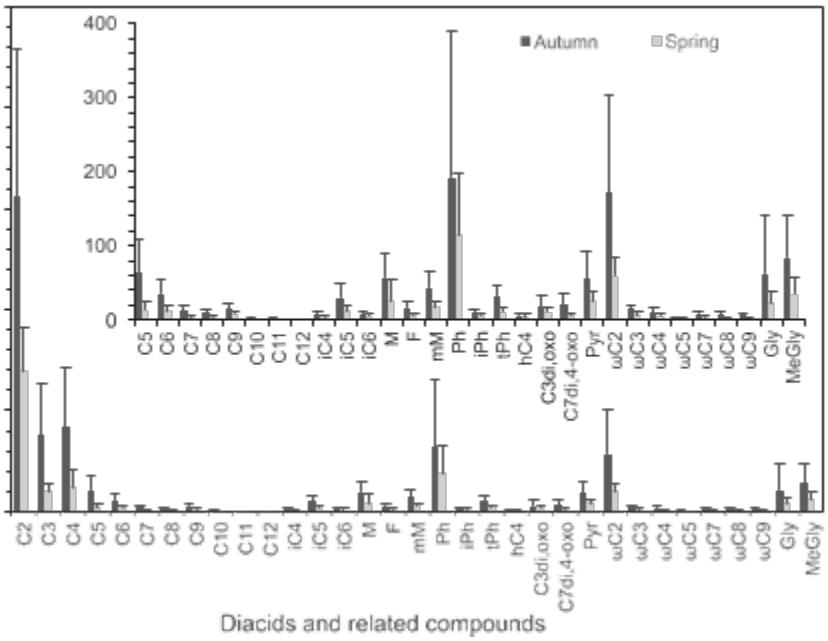

Fig. 2. Molecular distributions of dicarboxylic acids and related compounds in cloud waters collected over Mt. TMS, Hong Kong. The inner plot shows the concentrations of longer-chain saturated diacids (C_5–C_{12}), branched diacids, unsaturated diacids, multifunctional diacids, oxoacids and α-dicarbonyls, especially. See Table 1 for abbreviations

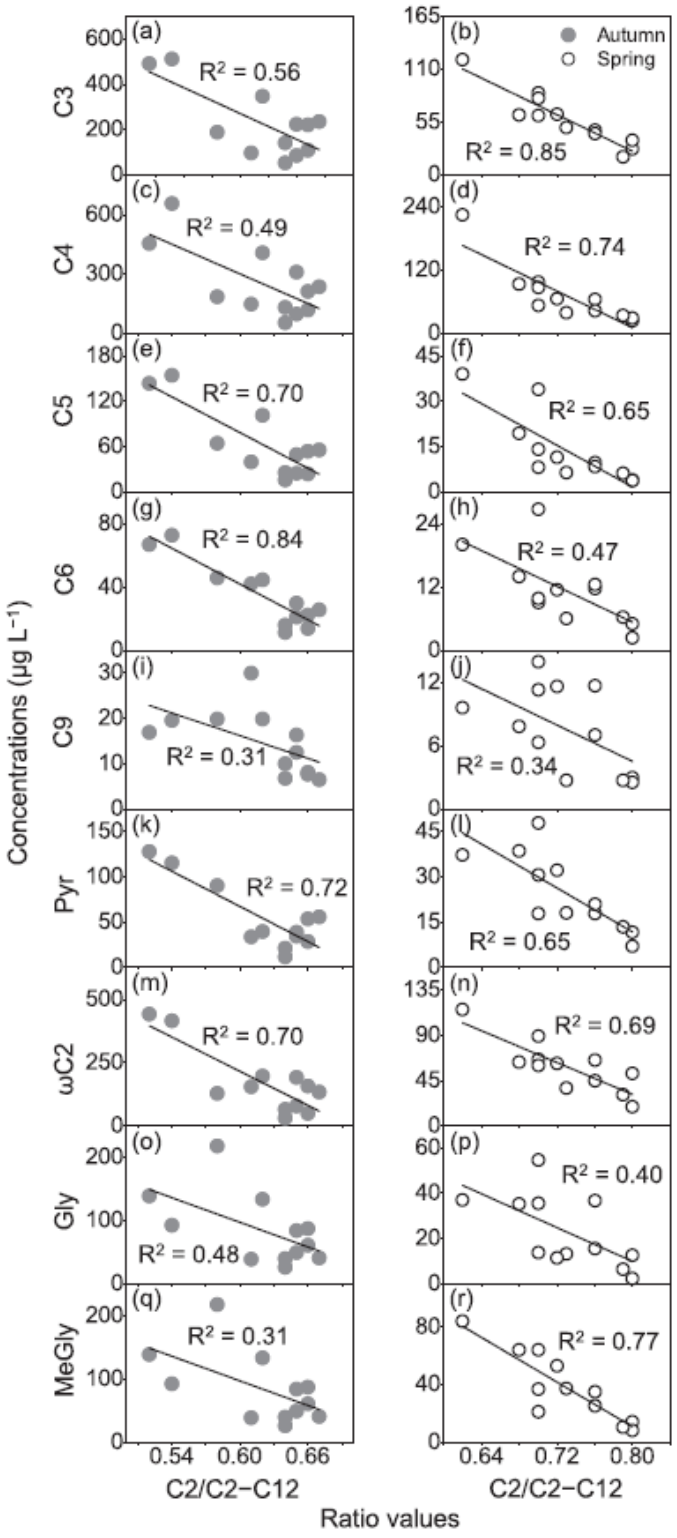

453

454 Fig. 3. Linear relationships for C_2/C_2–C_{12} with diacids and related compounds in autumn

455 and spring in cloud at Mt. TMS.

456

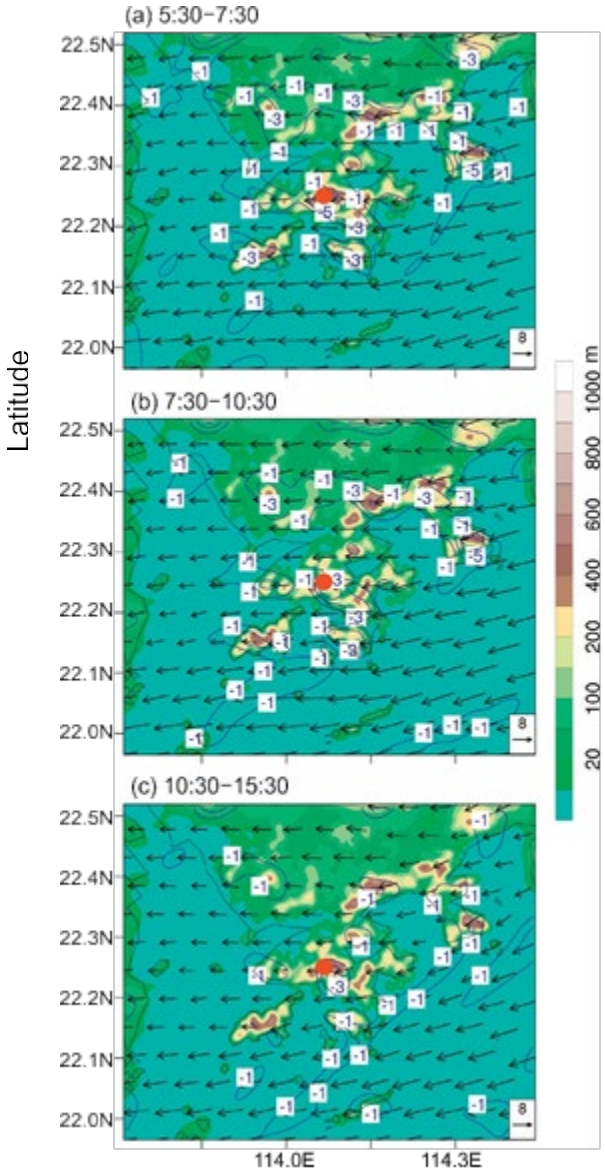

457

458 ig. 4. The divergence field (blue lines, units: 10^{-4} s^{-1}) and wind field (vector, units: m s^{-1}) of
459 Nov09#1 during 5:30–13:00 at Mt. TMS (red point, 957 m a.s.l.), and the levels of contour lines
460 are −1, −3 and −5, respectively. (For interpretation of the references to colour in this figure legend,
461 the reader is referred to the web version of this article.)

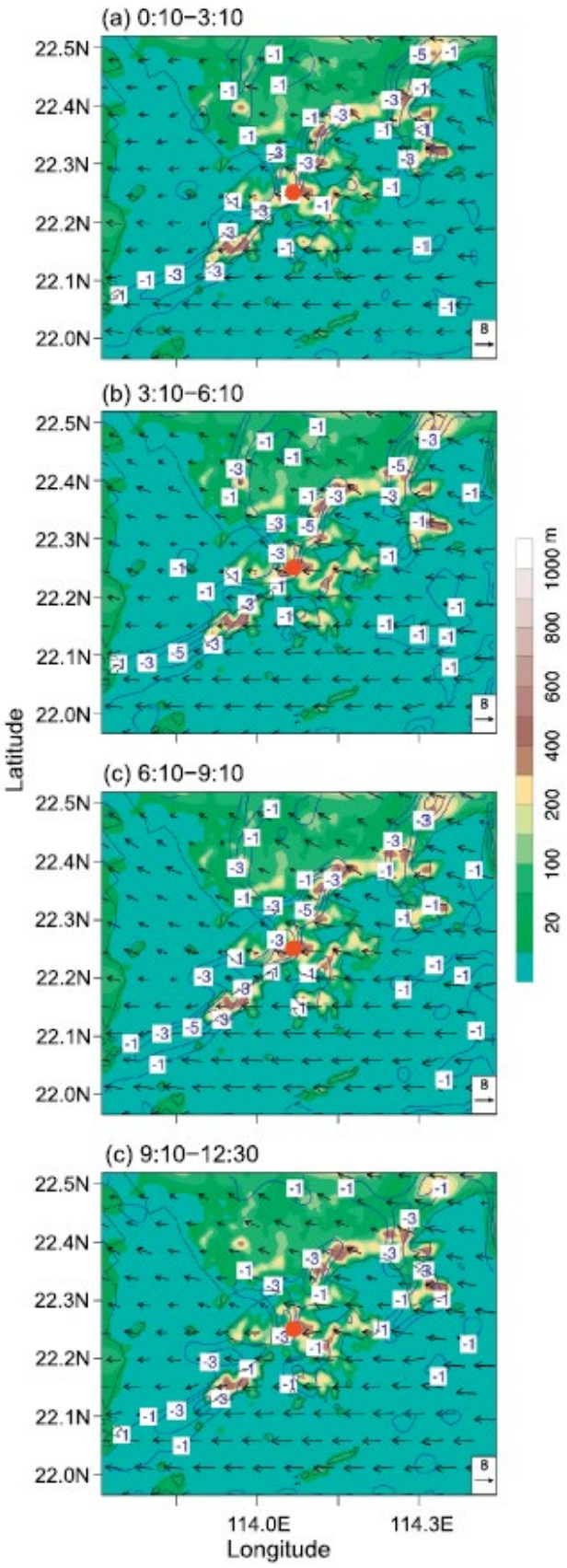
(a) 0:10−3:10
(b) 3:10−6:10
(c) 6:10−9:10
(c) 9:10−12:30
22.5N
22.4N
22.3N
22.2N
22.1N
22.0N
Latitude
114.0E
114.3E
Longitude
1000 m
800
600
400
200
100
20

462

Fig. 5. The divergence field (blue lines, units: 10^{-4} s^{-1}) and wind field (vector, units: m s^{-1}) of Nov16#2 during 0:10–12:30 at Mt. TMS (red point, 957 m a.s.l.), and the levels of contour lines are −1, −3 and −5, respectively. (For interpretation of the references to colour in this figure legend, the reader is referred to the web version of this article.)

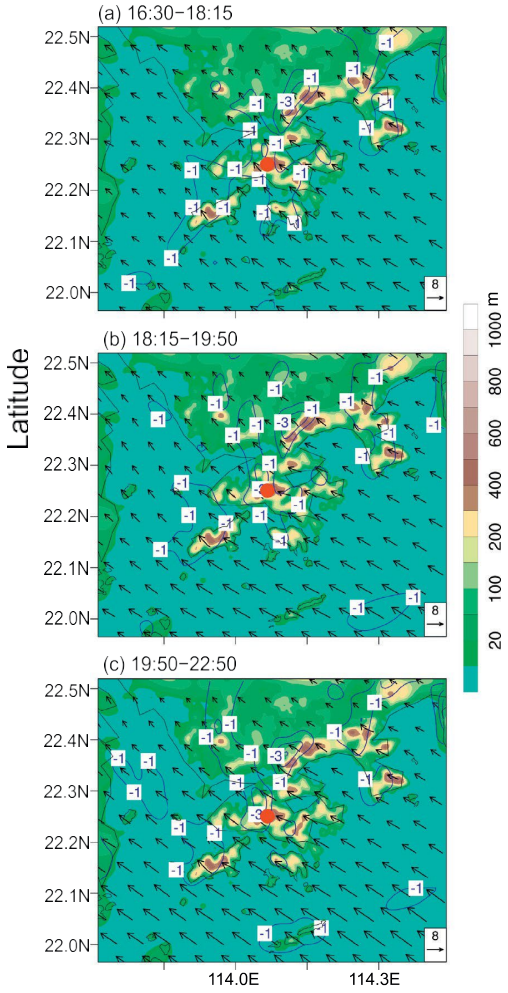

Fig. 6. The divergence field (blue lines, units: 10^{-4} s^{-1}) and wind field (vector, units: m s^{-1}) of Nov18#3 during 16:30–22:50 at Mt. TMS (red point, 957 m a.s.l.), and the levels of contour lines are −1, −3 and −5, respectively. (For interpretation of the references to colour in this figure legend, the reader is referred to the web version of this article.)

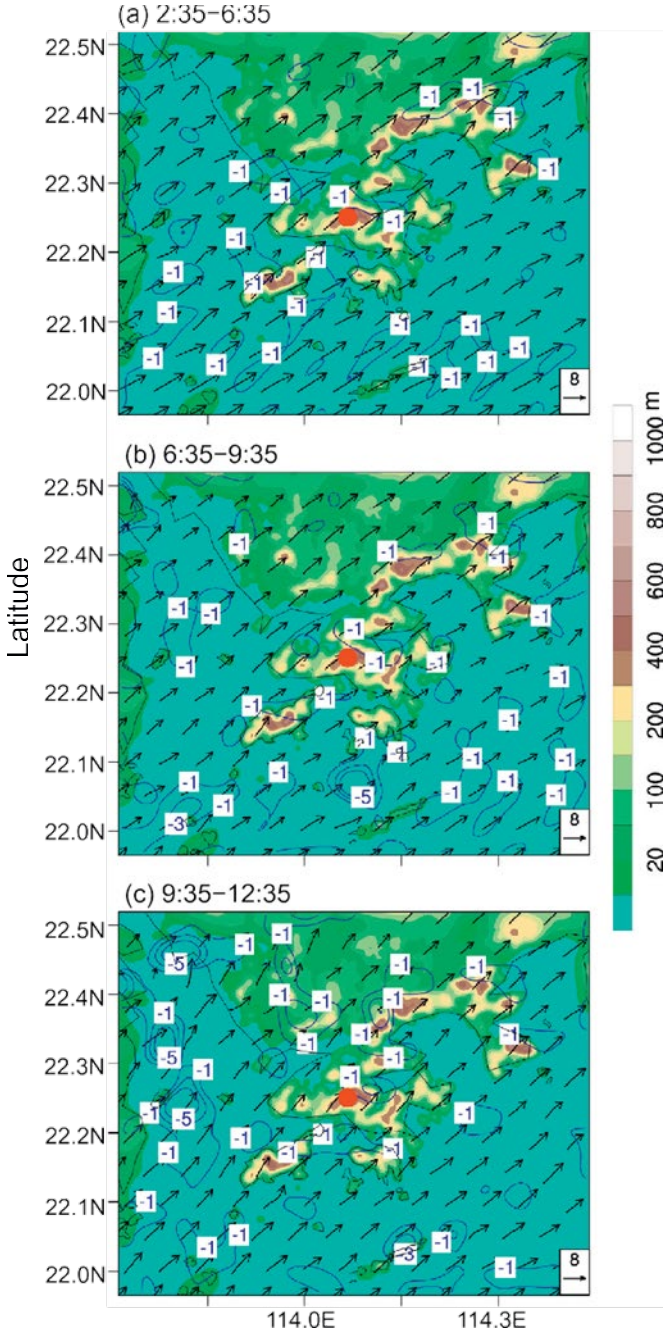

Fig. 7. The divergence field (blue lines, units: 10^{-4} s^{-1}) and wind field (vector, units: m s^{-1}) of Apr21#4 during 2:30–12:30 at Mt. TMS (red point, 957 m a.s.l.), and the levels of contour lines are −1, −3 and −5, respectively. (For interpretation of the references to colour in this figure legend, the reader is referred to the web version of this article.)

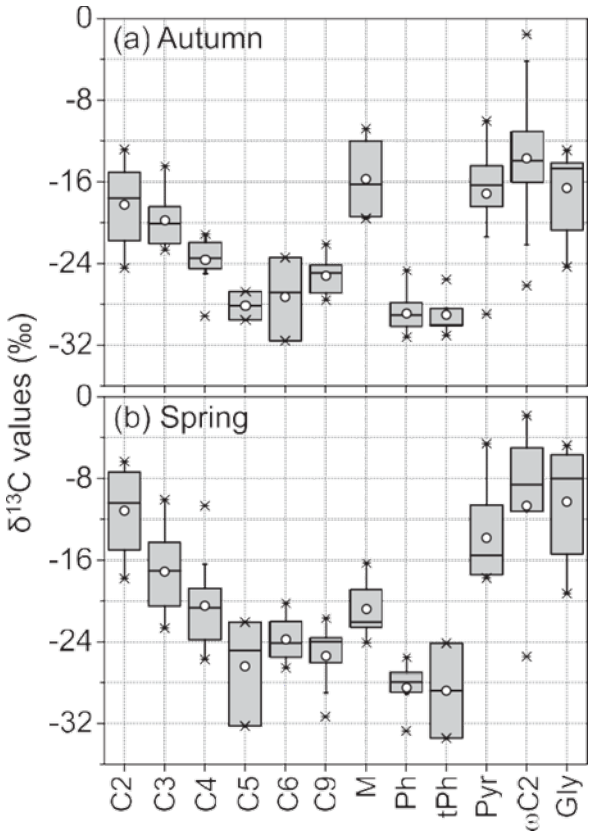

478

479 Fig. 9. Box plot of the δ13C values of dicarboxylic acids and related compounds. Small circles
480 represent the mean values.

481

482

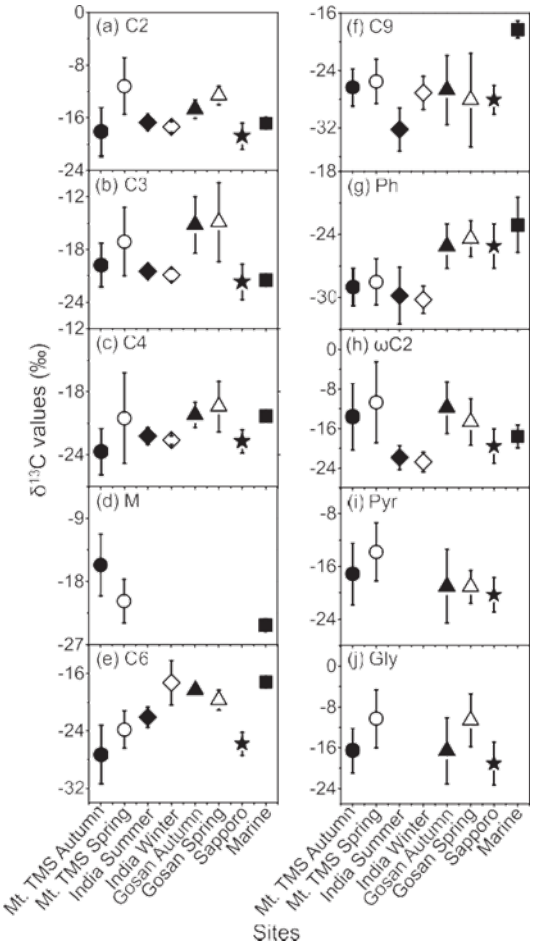

Fig. 10. Mean $\delta^{13}C$ values of dicarboxylic acids and related compounds in Mt. TMS cloud waters. Data in atmospheric aerosols collected from tropical India (Pavuluri et al., 2011), Sapporo (Aggarwal and Kawamura, 2008), Gosan, Jeju Island (Zhang et al., 2016b), and remote marine regions (Wang and Kawamura, 2006) are also plotted. The bars represent the standard variations (±SD) in the $\delta^{13}C$ values.

REFERENCES

Aggarwal, S.G., Kawamura, K., 2008. Molecular distributions and stable carbon isotopic compositions of dicarboxylic acids and related compounds in aerosols from Sapporo, Japan: implications for photochemical aging during long-range atmospheric trans- port. J. Geophys. Res. 113.

497 Akagi, S.K., Yokelson, R.J., Wiedinmyer, C., Alvarado, M.J., 2011. Emission factors for open and
498 domestic biomass burning for use in atmospheric models. Atmos. Chem. Phys. 11, 4039–4072.

499 Andreae, M., Rosenfeld, D., 2008. Aerosol–cloud–precipitation interactions. Part 1. The na- ture
500 and sources of cloud-active aerosols. Earth-Sci. Rev. 89, 13–41.

501 Andreae, M.O., 1983. Soot carbon and excess fine potassium: long-range transport of combustion-
502 derived aerosols. Science 220, 1148–1151.

503 Ballentine, D.C., Macko, S.A., Turekian, V.C., 1998. Variability of stable carbon isotopic
504 compositions in individual fatty acids from combustion of C4 and C3 plants: implica- tions for
505 biomass burning. Chem. Geol. 152, 151–161.

506 Bilde, M., Barsanti, K., Booth, M., Cappa, C.D., Donahue, N.M., Emanuelsson, E.U.,
507 McFiggans, G., Krieger, U.K., Marcolli, C., Topping, D., Ziemann, P., Barley, M., Clegg, S.,
508 Dennis-Smither, B., Hallquist, M., Hallquist, Å.M., Khlystov, A., Kulmala, M., Mogensen,
509 D., Percival, C.J., Pope, F., Reid, J.P., Ribeiro da Silva, M.A.V., Rosenoern, T., Salo, K., Soonsin,
510 V.P., Yli-Juuti, T., Prisle, N.L., Pagels, J., Rarey, J., Zardini, A.A., Riipinen, I., 2015.
511 Saturation vapor pressures and transition enthalpies of low- volatility organic molecules of
512 atmospheric relevance: from dicarboxylic acids to complex mixtures. Chem. Rev. 115, 4115–4156.

513 Cao, J.J., Lee, S.C., Ho, K.F., Zhang, X.Y., Zou, S.C., Fung, K., Chow, J.C., Watson, J.G., 2003.

514 Characteristics of carbonaceous aerosol in Pearl River Delta region, China during 2001 winter
515 period. Atmos. Environ. 37, 1451–1460.

516 Carlton, A.G., Turpin, B.J., Lim, H.J., Altieri, K.E., Seitzinger, S., 2006. Link between isoprene
517 and secondary organic aerosol (SOA): pyruvic acid oxidation yields low volatility or- ganic acids
518 in clouds. Geophys. Res. Lett. 33, 272–288.

519 Carlton, A.G., Turpin, B.J., Altieri, K.E., Seitzinger, S., Reff, A., Lim, H.-J., Ervens, B., 2007. At-
520 mospheric oxalic acid and SOA production from glyoxal: results of aqueous photoox- idation
521 experiments. Atmos. Environ. 41, 7588–7602.

522 Carlton, A.G., Wiedinmyer, C., Kroll, J.H., 2009. A review of secondary organic aerosol (SOA)
523 formation from isoprene. Atmos. Chem. Phys. 9, 4987–5005.

524 Chan, L.Y., Chan, C.Y., Qin, Y., 2010. Surface ozone pattern in Hong Kong. J. Appl. Meteorol.

525 37, 1153–1165.

526 Charbouillot, T., Gorini, S., Voyard, G., Parazols, M., Brigante, M., Deguillaume, L., Delort, A.-
527 M., Mailhot, G., 2012. Mechanism of carboxylic acid photooxidation in atmospheric aqueous
528 phase: formation, fate and reactivity. Atmos. Environ. 56, 1–8.

529 Chen, F., Kusaka, H., Bornstein, R., J., C., Grimmond, C.S.B., Grossman-Clarke, S., Loridan, T.,
530 Manning, K.W., Martilli, A., Miao, S., 2011. The integrated WRF/urban modelling sys- tem:
531 development, evaluation, and applications to urban environmental problems. Int. J. Climatol. 31,
532 273–288.

Chung, K.K., Chan, J.C.L., Ng, C.N., Lam, K.S., Wang, T., 1999. Synoptic conditions associated with high carbon monoxide episodes at a coastal station in Hong Kong. Atmos. Envi- ron. 33, 3087–3095.

Dabek-Zlotorzynska, E., Aranda-Rodriguez, R., Graham, L., 2005. Capillary electrophoresis determinative and GC-MS confirmatory method for water-soluble organic acids in airborne particulate matter and vehicle emission. J. Sep. Sci. 28, 1520–1528.

Dall'Osto, M., Harrison, R.M., Coe, H., Williams, P., 2009. Real-time secondary aerosol formation during a fog event in London. Atmos. Chem. Phys. 9, 2459–2469.

Demoz, B.B., Jr, J.L.C., Jr, B.C.D., 1996. On the caltech active strand cloudwater collectors.

Atmos. Res. 41, 47–62.

Ding, Y., 2005. Advanced Synoptic Science. China Meteorological Press 7.

Ding, Y., Si, D., Liu, Y., Zunya, Wang, Li, Y., Zhao, L., Yafang, S., 2018. On the characteristics, driving forces and inter-decadal variability of the east Asian summer monsoon. Chin.

J. Atmos. Sci. 42, 533–558 in Chinese.

Done, J., Davis, C.A., Weisman, M., 2004. The next generation of NWP: explicit forecasts of convection using the weather research and forecasting (WRF) model. Atmos. Sci. Lett. 5, 110–117.

Dudhia, J., 1989. Numerical study of convection observed during the winter monsoon experiment using a esoscale two-dimensional model. J. Atmos. Sci. 46, 3077–3107.

Ervens, B., Volkamer, R., 2010. Glyoxal processing by aerosol multiphase chemistry: to- wards a kinetic modeling framework of secondary organic aerosol formation in aque- ous particles. Atmos. Chem. Phys. 10, 12371–12431.

Ervens, B., Feingold, G., Frost, G.J., Kreidenweis, S.M., 2004. A modeling study of aqueous production of dicarboxylic acids: 1. Chemical pathways and speciated organic mass production. J. Geophys. Res. Atmos. 109.

Fang, J., Kawamura, K., Ishimura, Y., Matsumoto, K., 2002. Carbon isotopic composition of fatty acids in the marine aerosols from the western North Pacific: implication for the source and atmospheric transport. Environ. Sci. Technol. 36, 2598.

Fick, J., Nilsson, C., Andersson, B., 2004. Formation of oxidation products in a ventilation system. Atmos. Environ. 38, 5895–5899.

Fraser, M., Cass, G., Simoneit, B., 2003. Air quality model evaluation data for organics. 6.

C3-C24 organic acids. Environ. Sci. Technol. 37, 446–453.

Gioda, A., Mayol-Bracero, O.L., Reyes-Rodriguez, G.J., Santos-Figueroa, G., Collett Jr, J.L., 2008. Water-soluble organic and nitrogen levels in cloud and rainwater in a back- ground marine environment under influence of different air masses. J. Atmos. Chem. 61, 85–99.

569 Guo, H., So, K.L., Simpson, I.J., Barletta, B., Meinardi, S., Blake, D.R., 2007. C1-C8 volatile or-
570 ganic compounds in the atmosphere of Hong Kong: overview of atmospheric pro- cessing and
571 source apportionment. Atmos. Environ. 41, 1456–1472.

572 Hamilton, J.F., Lewis, A.C., Reynolds, J.C., Carpenter, L.J., Lubben, A., 2006. Investigat- ing the
573 composition of organic aerosol resulting from cyclohexene ozonolysis: low molecular weight and
574 heterogeneous reaction products. Atmos. Chem. Phys. 6, 4973–4984.

575 Hatakeyama, S., Ohno, M., Weng, J., Takagi, H., Akimoto, H., 1987. Mechanism for the for-
576 mation of gaseous and particulate products from ozone-cycloalkene reactions in air. Environ. Sci.
577 Technol. 21, 52–57.

578 Hegg, D.A., Gao, S., Jonsson, H., 2002. Measurements of selected dicarboxylic acids in ma- rine
579 cloud water. Atmos. Res. 62, 1–10.

580 Hennigan, C.J., Westervelt, D.M., Riipinen, I., Engelhart, G.J., Lee, T., Collett, J.L., Pandis, S.N.,
581 Adams, P.J., Robinson, A.L., 2012. New particle formation and growth in biomass burning plumes:
582 an important source of cloud condensation nuclei. Geophys. Res. Lett. 39.

583 Herckes, P., Valsaraj, K.T., Collett, J.L., 2013. A review of observations of organic matter in fogs
584 and clouds: origin, processing and fate. Atmos. Res. 132-133, 434–449.

585 Ho, K.F., Lee, S.C., Cao, J.J., Kawamura, K., Watanabe, T., Cheng, Y., Chow, J.C., 2006. Dicar-
586 boxylic acids, ketocarboxylic acids and dicarbonyls in the urban roadside area of Hong Kong.
587 Atmos. Environ. 40, 3030–3040.

588 Ho, K.F., Ho, S.S.H., Lee, S.C., Kawamura, K., Zou, S.C., Cao, J.J., Xu, H.M., 2011. Summer and
589 winter variations of dicarboxylic acids, fatty acids and benzoic acid in PM2.5 in Pearl Delta river
590 region, China. Atmos. Chem. Phys. 10, 26677–26703.

591 Huang, R.-J., Zhang, Y., Bozzetti, C., Ho, K.-F., Cao, J.-J., Han, Y., Daellenbach, K.R., Slowik,
592 J.G., Platt, S.M., Canonaco, F., 2014. High secondary aerosol contribution to particulate pollution
593 during haze events in China. Nature 514, 218–222.

594 Hwang, I., Hopke, P., 2007. Estimation of source apportionment and potential source locations of
595 PM2.5 at a west coastal IMPROVE site. Atmos. Environ. 41, 506–518. Joos, F., Baltensperger,
596 U., 1991. A field study on chemistry, S(IV) oxidation rates and ver-

597 tical transport during fog conditions. Atmos. Environ. Part A 25, 217–230.

598 Kain, J.S., 2004. The kain fritsch convective parameterization: an update. J. Appl. Meteorol.

599 43, 170–181.

600 Kautzman, K.E., Surratt, J.D., Chan, M.N., Chan, A.W.H., Hersey, S.P., Chhabra, P.S., Dalleska,
601 N.F., Wennberg, P.O., Flagan, R.C., Seinfeld, J.H., 2010. Chemical composition of gas- and
602 aerosol-phase products from the photooxidation of naphthalene. J. Phys. Chem. A 114, 913–934.

603 Kawamura, K., Bikkina, S., 2016. A review of dicarboxylic acids and related compounds in
604 atmospheric aerosols: molecular distributions, sources and transformation. Atmos. Res. 170, 140–
605 160.

606 Kawamura, K., Gagosian, R., 1987. Implications of ω-oxocarboxylic acids in the remote marine
607 atmosphere for photo-oxidation of unsaturated fatty acids. Nature 325, 330–332.

608 Kawamura, K., Ikushima, K., 1993. Seasonal changes in the distribution of dicarboxylic acids in
609 the urban atmosphere. Environ. Sci. Technol. 27, 2227–2235.

610 Kawamura, K., Kaplan, I.R., 1987. Motor exhaust emissions as a primary source for dicarboxylic
611 acids in Los Angeles ambient air. Environ. Sci. Technol. 21, 105–110.

612 Kawamura, K., Pavuluri, C.M., 2010. New directions: need for better understanding of plastic
613 waste burning as inferred from high abundance of terephthalic acid in south Asian aerosols. Atmos.
614 Environ. 44, 5320–5321.

615 Kawamura, K., Sakaguchi, F., 1999. Molecular distributions of water soluble dicarboxylic acids
616 in marine aerosols over the Pacific Ocean including tropics. J. Geophys. Res. Atmos. 104, 3501–
617 3509.

618 Kawamura, K., Kasukabe, H., Barrie, L.A., 1996. Source and reaction pathways of dicarbox- ylic
619 acids, ketoacids and dicarbonyls in arctic aerosols: one year of observations. Atmos. Environ. 30,
620 1709–1722.

621 Kawamura, K., Watanabe, T., Chem, A., 2004. Determination of stable carbon isotopic
622 compositions of low molecular weight dicarboxylic acids and ketocarboxylic acids in atmospheric
623 aerosol and snow samples. Anal. Chem. 76, 5762–5768.

624 Kawamura, K., Kasukabe, H., Barrie, L.A., 2010. Secondary formation of water-soluble or- ganic
625 acids and α-dicarbonyls and their contributions to total carbon and water- soluble organic carbon:
626 photochemical aging of organic aerosols in the Arctic spring.

627 J. Geophys. Res. Atmos. 115.

628 Kawamura, K., Tachibana, E., Okuzawa, K., Aggarwal, S., Kanaya, Y., Wang, Z., 2013. High
629 abundances of water-soluble dicarboxylic acids, ketocarboxylic acids and α- dicarbonyls in
630 the mountaintop aerosols over the North China plain during wheat burning season. Atmos. Chem.
631 Phys. 13, 8285–8302.

632 Keene, W.C., Pszenny, A.A.P., Galloway, J.N., Hawley, M.E., 1986. Sea-salt corrections and
633 interpretation of constituent ratios in marine precipitation. J. Geophys. Res. Atmos. 91, 6647–6658.

634 Kessler, E., 1995. On the continuity and distribution of water substance in atmospheric circulations.
635 Atmos. Res. 38, 109–145.

636 Khwaja, H.A., Brudnoy, S., Husain, L., 1995. Chemical characterization of three summer cloud
637 episodes at whiteface mountain. Chemosphere 31, 3357–3381.

638 Kleindienst, T., Jaoui, M., Lewandowski, M., Offenberg, J., Docherty, K., 2012. The formation of
639 SOA and chemical tracer compounds from the photooxidation of naphthalene and its methyl
640 analogs in the presence and absence of nitrogen oxides. Atmos. Chem. Phys. 12, 8711–8726.

641 Kumar, S., Aggarwal, S.G., Gupta, P.K., Kawamura, K., 2015. Investigation of the tracers for
642 plastic-enriched waste burning aerosols. Atmos. Environ. 108, 49–58.

643 Lee, S.C., Ho, K.F., Chan, L.Y., Zielinska, B., Chow, J.C., 2001. Polycyclic aromatic hydrocar-
644 bons (PAHs) and carbonyl compounds in urban atmosphere of Hong Kong. Atmos. Environ. 35,
645 5949–5960.

646 Lee, S.C., Chiu, M.Y., Ho, K.F., Zou, S.C., Wang, X., 2002. Volatile organic compounds (VOCs)
647 in urban atmosphere of Hong Kong. Chemosphere 48, 375–382.

648 Legrand, M., Angelis, M.D., 1996. Light carboxylic acids in Greenland ice: a record of past forest
649 fires and vegetation emissions from the boreal zone. J. Geophys. Res. Atmos. 101, 4129–4145.

650 Lei, W., Li, G., Molina, L.T., 2012. Modeling the impacts of biomass burning on air quality in and
651 around Mexico City. Atmos. Chem. Phys. 12, 2299–2319.

652 Li, D., Bou-Zeid, E., 2013. Synergistic interactions between urban heat islands and heat waves:
653 the impact in cities is larger than the sum of its parts. J. Appl. Meteorol. Climatol. 52, 2051–2064.

654 Liljestrand, H.M., Morgan, J.J., 1981. Spatial variations of acid precipitation in southern Cal-
655 ifornia. Environ. Sci. Technol. 15, 333.

656 Lim, H.-J., Carlton, A.G., Turpin, B.J., 2005. Isoprene forms secondary organic aerosol through
657 cloud processing: model simulations. Environ. Sci. Technol. 39, 4441–4446.

658 Lim, Y.B., Tan, Y., Perri, M.J., Seitzinger, S.P., Turpin, B.J., 2010. Aqueous chemistry and its
659 role in secondary organic aerosol (SOA) formation. Atmos. Chem. Phys. 10, 10521–10539.

660 Limbeck, A., Puxbaum, H., 2000. Dependence of in-cloud scavenging of polar organic aero- sol
661 compounds on the water solubility. J. Geophys. Res. Atmos. 105, 19857–19867.

662 Liu, H., Chan, J.C.L., 2002a. An investigation of air-pollutant patterns under sea–land breezes
663 during a severe air-pollution episode in Hong Kong. Atmos. Environ. 36, 591–601.

664 Liu, H.P., Chan, J.C.L., 2002b. Boundary layer dynamics associated with a severe air- pollution
665 episode in Hong Kong. Atmos. Environ. 36, 2013–2025.

666 Löflund, M., Kasper-Giebl, A., Schuster, B., Giebl, H., Hitzenberger, R., Puxbaum, H., 2002.
667 Formic, acetic, oxalic, malonic and succinic acid concentrations and their contribution to organic
668 carbon in cloud water. Atmos. Environ. 36, 1553–1558.

669 Louie, P.K.K., Watson, J.G., Chow, J.C., Chen, A., Sin, D.W.M., Lau, A.K.H., 2005. Seasonal
670 characteristics and regional transport of PM2.5 in Hong Kong. Atmos. Environ. 39, 1695–1710.

671 Markowski, P., Richardson, Y., 2010. Mesoscale Meteorology in Midlatitudes. Wiley- Blackwell.

672 Mass, C., 1981. Topographically forced convergence in Western Washington state. Mon.

673 Wea. Rev. 109, 1335.

674 Mass, C.F., Dempsey, D.P., 1985. A topographically forced convergence line in the Lee of the
675 Olympic Mountains. Mon. Wea. Rev. 113, 659.

676 Matsumoto, K., Kawamura, K., Uchida, M., Shibata, Y., 2007. Radiocarbon content and sta- ble
677 carbon isotopic ratios of individual fatty acids in subsurface soil: implication for selective
678 microbial degradation and modification of soil organic matter. Geochem. J. 41, 483–492.

McNeill, V.F., 2015. Aqueous organic chemistry in the atmosphere: sources and chemical processing of organic aerosols. Environ. Sci. Technol. 49, 1237–1244.

Mlawer, E.J., Taubman, S.J., Brown, P.D., Iacono, M.J., Clough, S.A., 1997. Radiative transfer for inhomogeneous atmospheres: RRTM, a validated correlated-k model for the longwave. J. Geophys. Res. Atmos. 102, 16663–16682.

Mochida, M., Umemoto, N., Kawamura, K., Lim, H.-J., Turpin, B.J., 2007. Bimodal size distributions of various organic acids and fatty acids in the marine atmosphere: influence of anthropogenic aerosols, Asian dusts, and sea spray off the coast of East Asia.

J. Geophys. Res. 112.

Müller, C., Iinuma, Y., Böge, O., Herrmann, H., 2007. Applications of CE-ESI-MS/MS analysis to structural elucidation of methylenecyclohexane ozonolysis products in the particle phase. Electrophoresis 28, 1364–1370.

Myriokefalitakis, S., Vrekoussis, M., Tsigaridis, K., Wittrock, F., Richter, A., Brühl, C., Volkamer, R., Burrows, J., Kanakidou, M., 2008. The influence of natural and anthropo- genic secondary sources on the glyoxal global distribution. Atmos. Chem. Phys. 8, 4965–4981.

Na, K., Kim, Y.P., Moon, K.C., 2003. Diurnal characteristics of volatile organic compounds in the Seoul atmosphere. Atmos. Environ. 37, 733–742.

Narukawa, M., Kawamura, K., Takeuchi, N., Nakajima, T., 1999. Distribution of dicarboxylic acids and carbon isotopic compositions in aerosols from 1997 Indonesian forest fires. Geophys. Res. Lett. 26, 3101–3104.

Narukawa, M., Kawamura, K., Li, S.M., Bottenheim, J.W., 2002. Dicarboxylic acids in the Arctic aerosols and snowpacks collected during ALERT 2000. Atmos. Environ. 36, 2491–2499.

Noble, E., Druyan, L.M., Fulakeza, M., 2013. The sensitivity of WRF daily summertime simulations over West Africa to alternative parameterizations. Part I: African wave circu- lation. Mon. Wea. Rev. 142, 1588–1608.

Pavuluri, C.M., Kawamura, K., 2012. Evidence for 13-carbon enrichment in oxalic acid via iron catalyzed photolysis in aqueous phase. Geophys. Res. Lett. 39, 3802.

Pavuluri, C.M., Kawamura, K., Swaminathan, T., Tachibana, E., 2011. Stable carbon isotopic compositions of total carbon, dicarboxylic acids and glyoxylic acid in the tropical Indian aerosols: implications for sources and photochemical processing of organic aerosols. J. Geophys. Res. 116.

Prenni, A.J., DeMott, P.J., Kreidenweis, S.M., Sherman, D.E., Russell, L.M., Ming, Y., 2001. The effects of low molecular weight dicarboxylic acids on cloud formation. J. Phys. Chem. A 105, 11240–11248.

Rinaldi, M., Decesari, S., Carbone, C., Finessi, E., Fuzzi, S., Ceburnis, D., O'Dowd, C.D., Sciare, J., Burrows, J.P., Vrekoussis, M., Ervens, B., Tsigaridis, K., Facchini, M.C., 2011. Evidence of a natural marine source of oxalic acid and a possible link to glyoxal. J. Geophys. Res. Atmos. 116, 971–978.

Rogge, W.F., Hildemann, L.M., Mazurek, M.A., Cass, G.R., Simoneit, B.R., 1993. Sources of fine organic aerosol. 2. Noncatalyst and catalyst-equipped automobiles and heavy- duty diesel trucks. Environ. Sci. Technol. 27, 636–651.

Rolph, G., Stein, A., Stunder, B., 2017. Real-time environmental applications and display sYstem: READY. Environ. Model. Softw. 95, 210–228.

Schwartz, C.S., 2014. Reproducing the September 2013 record-breaking rainfall over the Colorado front range with high-resolution WRF forecasts. Wea. Forecasting 29, 393–402.

Skamarock, W.C., 2008. A description of the advanced research WRF version 3. Ncar Tech- nical 113, 7–25.

Sullivan, A.P., Hodas, N., Turpin, B.J., Skog, K., Keutsch, F.N., Gilardoni, S., Paglione, M., Rinaldi, M., Decesari, S., Facchini, M.C., 2015. Evidence for ambient dark aqueous SOA formation in the Po Valley, Italy. Atmos. Chem. Phys. 15, 35485–35521.

Tan, Y., Carlton, A.G., Seitzinger, S.P., Turpin, B.J., 2010. SOA from methylglyoxal in clouds and wet aerosols: measurement and prediction of key products. Atmos. Environ. 44, 5218–5226.

Tedetti, M., Kawamura, K., Charrière, B., Chevalier, N., Sempéré, R., 2006. Determination of low molecular weight dicarboxylic and ketocarboxylic acids in seawater samples. Anal. Chem. 78, 6012–6018.

Turekian, V.C., Macko, S.A., Keene, W.C., 2003. Concentrations, isotopic compositions, and sources of size-resolved, particulate organic carbon and oxalate in near-surface ma- rine air at Bermuda during spring. J. Geophys. Res. 108, 347–362.

Van Pinxteren, D., Wadinga Fomba, K., Mertes, S., Müller, K., Spindler, G., Schneider, J., Lee, T., Collett, J.L., Herrmann, H., 2016. Cloud water composition during HCCT- 2010: scavenging efficiencies, solute concentrations, and droplet size depen- dence of inorganic ions and dissolved organic carbon. Atmos. Chem. Phys. 16, 3185–3205.

Voisin, D., Legrand, M., Chaumerliac, N., 2000. Scavenging of acidic gases (HCOOH, CH3COOH, HNO3, HCl, and SO2) and ammonia in mixed liquid-solid water clouds at the Puy de Dôme mountain (France). J. Geophys. Res. Atmos. 105, 6817–6835.

Volkamer, R., Platt, U., Wirtz, K., 2001. Primary and secondary glyoxal formation from ar- omatics: experimental evidence for the bicycloalkyl-radical pathway from benzene, toluene, and p-xylene. J. Phys. Chem. A 105, 7865–7874.

Wang, G., Kawamura, K., Cheng, C., Li, J., Cao, J., Zhang, R., Zhang, T., Liu, S., Zhao, Z., 2012. Molecular distribution and stable carbon isotopic composition of dicarboxylic acids, ketocarboxylic acids, and α-dicarbonyls in size-resolved atmospheric particles from Xi'an City, China. Environ. Sci. Technol. 46, 4783–4791.

Wang, H., Kawamura, K., 2006. Stable carbon isotopic composition of low-molecular- weight dicarboxylic acids and ketoacids in remote marine aerosols. J. Geophys. Res. Atmos. 111.

Wang, T., Lam, K.S., Lee, A.S.Y., Pang, S.W., Tsui, W.S., 1998. Meteorological and chemical characteristics of the photochemical ozone episodes observed at cape D'Aguilar in Hong Kong. J. Appl. Meteorol. 37, 1167–1178.

Wang, T., Tham, Y.J., Xue, L., Li, Q., Zha, Q., Wang, Z., Poon, S.C.N., Dubé, W.P., Blake, D.R., Louie, P.K.K., Luk, C.W.Y., Tsui, W., Brown, S.S., 2016. Observations of nitryl chloride and modeling its source and effect on ozone in the planetary boundary layer of south- ern China. J. Geophys. Res. Atmos. 121, 2476–2489.

Widory, D., Roy, S., Moullec, Y.L., Goupil, G., Cocherie, A., Guerrot, C., 2004. The origin of atmospheric particles in Paris: a view through carbon and lead isotopes. Atmos. En- viron. 38, 953–961.

Zhang, Y.L., Kawamura, K., Cao, F., Lee, M., 2016b. Stable carbon isotopic compositions of low-molecular-weight dicarboxylic acids, oxocarboxylic acids, α-dicarbonyls, and fatty acids: implications for atmospheric processing of organic aerosols. J. Geophys. Res. Atmos. 121, 3707–3717.

Zhang, Y.-L., Kawamura, K., Agrios, K., Lee, M., Salazar, G., Szidat, S., 2016a. Fossil and non-fossil sources of organic and elemental carbon aerosols in the outflow from Northeast China. Environ. Sci. Technol. 50, 6284–6292.

Zhao, W., Kawamura, K., Yue, S., Wei, L., Ren, H., Yan, Y., Kang, M., Li, L., Ren, L., Lai, S., Li, J., Sun, Y., Wang, Z., Fu, P., 2018. Molecular distribution and compound-specific stable carbon isotopic composition of dicarboxylic acids, oxocarboxylic acids and α- dicarbonyls in PM2.5 from Beijing, China. Atmos. Chem. Phys. 18, 2749–2767